Stress measurement in East Asian lacquer thin films due to changes in relative humidity using phase shifting interferometry.

A. E. Elmahdy[a], P. D. Ruiz[a], R. D. Wildman[a], J. M. Huntley[a], S. Rivers[b],
[a]Wolfson School of Mechanical and Manufacturing Engineering, Loughborough University, Loughborough, LE11 3TU, UK
[b] Victoria and Albert Museum, London, UK SW7 2RL, UK

Abstract

We investigated the response of Japanese lacquer (*urushi*) to changes in environment conditions by examining the deflection of a glass substrate coated with a thin film of urushi when it was subjected to three different changes in humidity levels. This deflection was measured using phase shifting interferometry then related to the bending moment and in-plane stress developed in the system due to the expansion mismatch in the bilayer using Atkinson's formula. This was performed for aged and non-aged lacquers, at a range of relative humidities. Upon changing the humidities we observed rapidly changing stresses in the lacquers, which then showed evidence of relaxation over much longer timescales. Comparison of the behaviour of the aged and non-aged lacquers showed that both have the same response to changes in the humidity. During desorption, stresses were higher for the non-aged urushi films while during adsorption stresses were higher for the aged urushi films.

Key words: East Asian lacquer film, *urushi*, UV aging, phase shifting interferometer, coating/substrate bending, stress.

1. Introduction

Lacquers generally serve two functions. They can be used as a means of protecting an object, attempting to insulate it from the effects of the environment or alternatively they can be a medium for decoration. In some objects, of course, the lacquer may serve both purposes and an exquisite example of this is the use of natural lacquers, also known as *urushi* in Japan (Awazu *et al.* 1999; Kumanotani 1995; Lu *et al.* 2003; Ogawa *et al.* 1998a; Ogawa *et al.* 1998b), that have been used on Asian artifacts for centuries. The work described in this paper has been motivated by the need to

conserve the lacquer on the artifact known as the Mazarin Chest (Rivers 2003), currently held at the Victoria and Albert Museum. The Mazarin Chest is one of finest extant pieces of 17th Century Japanese *urushi* craftsmanship. Unfortunately, however, environmental conditions have taken their toll on the lacquer surface and conservators are faced with a number of questions regarding its repair. In the years since their manufacture, lacquers suffer from different kinds of damage as a result of storage and display in fluctuating environmental conditions, e.g. changing relative humidity, temperature and lighting. This can lead to discoloration and fading of the originally glossy lacquer surface as a result of the formation of micro-cracks on the surface.

One of the most common methods used for conservation of natural lacquer objects is to apply another layer of *urushi* (often diluted) to the damaged surface, with the effect of filling any holes or micro-cracks caused by damage to the original surface. Unfortunately, although tradition holds that this is generally a successful route, conservators do not know for sure whether this is the most effective method, or indeed, whether such a choice can lead to a negative long term impact.

In order to be able to answer questions regarding the efficacy of conservation methods, we must first understand that the lacquer is a complex, composite system that is affected by not only the environmental conditions, but by how it interacts with the object itself. The logical approach must then be to first establish the properties and response of *urushi* in isolation, before then proceeding to consider the interaction between various components of the system as a whole: environment, lacquer layers and object.

Key dependencies of the mechanical properties of *urushi* are the temperature, moisture content and ultra-violet exposure. All three have an effect on the "ageing" of the material and the duration of exposure to UV and elevated thermal conditions indicate strong history dependence. Therefore we can consider two types of effects, long term changes in the physics or the material structure, usually attributable to chemical changes due to moisture, elevated temperature or UV exposure; and reversible changes due to temperature and moisture content dependent material properties.

Ogawa *et al* (Ogawa *et al.* 1998a) investigated the effect of exposure to fluorescent lamps on the mechanical properties of East Asian lacquer films. The films were

exposed to light under three different conditions: uncovered, in a box of acrylic plates, and in a box of glass plates. Hardness was obtained using a hardness meter with a load of 25 g under a pressing time of 15 s and tensile tests were carried out using a tensile tester. They found that the hardness and the elastic modulus increased with exposure time, while the tensile strength and the elongation at break decreased with exposure time. They concluded that the increased hardness is related to a cross-linking reaction by the enzyme laccase over the whole region of the films. Other studies have shown that following exposure to UV radiation, the surface of *urushi* fades and becomes dull as light breaks down the molecular structure (Rivers 2003). Under magnification, one can see that the dull appearance is actually a network of micro-cracks that formed on the surface of the lacquerware.

Lacquer properties are also affected by the moisture levels within the material. Ogawa *et al* (Ogawa *et al.* 1998b) investigated the effect of water on mechanical properties of a film of constant thickness. A tensile test was carried out on 4 × 35 × 0.05 mm samples at a test speed of 2 $mm.min^{-1}$ and under various degrees of humidity ranging from 15% to 100%. They concluded that East Asian films had a tendency to toughen by water absorption, leading to an increase in the strain at break and a decrease in the elastic modulus. This behaviour was caused by water serving as a plasticizer. Conversely, East Asian films have a tendency to become brittle when the moisture is removed. Ogawa *et al* (Ogawa *et al.* 1998b) also investigated the changes to the relaxation modulus over a period of 100 hrs, using a dynamic viscoelastometer. The experiments were carried out under known temperature and humidity conditions, and it was found that the relaxation modulus of the film in a wet condition decreases rapidly with time.

Changes in the relative humidity can have a number of effects. Firstly, the moisture can accumulate at the interfaces between layers generating stresses or can act to reduce the adhesive strength of these interfaces. The result is that delamination can occur and the lacquer may eventually peel off from the object. Obataya *et al* (Obataya *et al.* 2002) demonstrated that moisture content significantly affected the viscoelastic properties of *urushi*. They used three lacquer films, clear, virgin and black. The clear and black lacquer films were kurome-treated lacquer whereas the virgin lacquer was an unrefined filtered sap. The black lacquer was coloured through a chemical reaction with 1% of iron powder. The water sorption of aged lacquer films was determined at

30 °C within the range of 10-90% relative humidity (RH). The moisture dependence of their storage modulus and the loss tangent (tanδ) were measured at 0.5 Hz and 30 °C within the range of 10-90% RH, using a viscoelastometer. The equilibrium moisture content (MC) of the virgin lacquer film was higher than that of the clear lacquer film over the RH range (10-90%), attributable to the hygroscopicity of polysaccharide aggregated during drying. Obataya *et al* found that the storage modulus decreased and the loss tangent (tanδ) increased with increasing moisture content for both clear and virgin lacquer films. Although the hygroscopicity of the virgin lacquer film was larger than that of the clear lacquer film, its storage modulus and the loss tangent (tanδ) were only nearly affected by moisture sorption.

Many other techniques have been used to observe and measure the response of coatings to changes in the environmental conditions (Francis *et al.* 2002; Withers *et al.* 2001). These techniques make use of relations between the physical or crystallographic parameters and the stress developed in the coatings. These techniques include X-ray diffraction, neutron diffraction, ultrasound, curvature measurements, nano-indentation and Raman/Fourier-Transform Infrared Spectroscopy. The physical principle of stress measurement by neutron diffraction is similar to those for the X-ray diffraction method. The greatest advantage that neutrons have over X-rays is the very large penetration depths that neutrons can achieve (Kandil *et al.* 2001; Lu 1996). Ultrasonic methods are based on the variation of the velocity of ultrasound waves travelling through a solid where this variation can be related to the stress state (Kandil *et al.* 2001; Lu 1996). Raman scattered light conveys information about a sample's physical state and chemical structure. Raman spectral lines shift linearly with hydrostatic stress and can be used to measure residual stresses (Cabié *et al.* 2004; Kim *et al.* 1998). However, it relies on spectral signatures of narrow bandwidth which are unfortunately absent in *urushi*. A number of authors have used the curvature method to determine residual stresses in thin films and the wide applicability and accuracy of this approach has shown it to be a very powerful method (Chen *et al.* 2003; Clyne *et al.* 1996; Klein 2000; Matejicek *et al.* 2003; Schafer *et al.* 1999; Tsui *et al.* 1997). In this paper we present a variant using phase shifting interferometry to determine small strains and stresses in urushi thin films (Tien *et al.* 2000).

It is clear that the behaviour of *urushi* is highly complex. It is a viscoelastic medium with evidence of thixotropy, with strong changes in its mechanical behaviour when

subjected to changes in moisture content and UV illumination. In order to formulate a predictive mechanical model for *urushi* that includes its constitutive relations, a comprehensive analysis of the response of *urushi* to changes in environmental conditions is still required in order to determine the precise nature of the relationship between stress, strain, moisture content and thermal and UV conditioning. Moreover, as the ultimate cause for the formation of surface micro-cracks is the surface stress, detailed measurements of the dependence of film stress with environmental conditions and for aged and non-aged films are required. In this paper, we present a methodology to achieve this and start by measuring the film stress as a function of changes in relative humidity using the curvature method. In Section 3 we describe our optically based experimental technique that allows us to determine small deformations of a substrate coated with a thin *urushi* film due to small changes in the environmental conditions. Finally, in Section 4 we compare the response of an *urushi* layer exposed to a substantial period of elevated temperatures and UV illumination to that of a non-aged layer.

2. Methodology

2.1 The Curvature Method

The curvature method, widely used for the determination of residual stresses in thin films, consists of measuring the deflection of a substrate plate due to stress build up in the film after this is deposited on the substrate. The deformation is usually a change in the curvature of the substrate depending on the tensile or compressive nature of the film stress. Under certain conditions, the substrate deflection field $\delta(x,y)$ and the average stress σ in the film are related by the following approximation, known as Atkinson's formula (Chen *et al.* 2003; Clyne *et al.* 1996; Klein 2000; Matejicek *et al.* 2003; Schafer *et al.* 1999; Tsui *et al.* 1997):

$$\sigma = \frac{t_s^3}{3t_f^2(1+t_s/t_f)}\frac{E_s}{(1-\nu_s)}\frac{\delta(r,\theta)}{r^2}, \qquad (1)$$

where E_s, ν_s and t_s are the Young's modulus, Poisson's ratio and thickness of the substrate respectively. t_f is the film thickness, assumed constant all over the substrate, whilst $r=(x^2+y^2)^{1/2}$ and $\theta=\tan^{-1}(y/x)$ are the polar coordinates of point (x,y) as shown in Fig. (1). It is worth noting that, provided certain conditions are satisfied, σ is independent of the Young's modulus and Poisson's ratio of the film, which makes

this method appealing for our purposes as these are unknown. The assumptions (Huang *et al.* 2006) used to derive Eq. (1) are that the

1. strains and rotations are infinitesimally small,
2. film/substrate thickness ratio is $t_f/t_s < 0.4$. When the thickness ratio $t_f/t_s << 0.1$, however, a simpler approximation can be used, known as Stoney's equation (Klein 2000; Schafer *et al.* 1999),
3. substrate and film materials are homogeneous, isotropic and linearly elastic,
4. the film is in plane stress, i.e., there are no appreciable stress gradients through the film thickness.

For our thin films, these assumptions are generally true. It is worth noting that although this technique was developed with the aim of measuring residual stresses, our concern in this paper is to measure the response of the average stress in *urushi* thin films due to changes in relative humidity. In order to achieve this with the curvature method, several requirements needed to be addressed. First, an appropriate film and substrate system has to be designed so that assumptions 1-4 are all met (see Section 2.1). Secondly, a highly sensitive method is required to measure the small deflections expected of the substrate (see Section 2.2). Finally, a chamber had to be built to enable full control over the system environment (see Section 3.2).

2.2 Non-contact deflection measurement using phase shifting interferometry

Phase Shifting Interferometry (PSI) is a well known optical technique that allows full-field, non-contact measurements of sub-micrometer deformations without sign ambiguities (Cheng *et al.* 1985; Malacara *et al.* 2005; Robinson 1993; Tien *et al.* 2000). These features make PSI an ideal candidate for measuring small substrate deflections.

When two beams that originate from a common light source are recombined after they have travelled optical paths that differ by no more than the coherence length of the source, they interfere and form a fringe pattern. This is usually recorded with a 2D detector array and can be described by the following intensity distribution,

$$I(x,y) = I_0(x,y) + I_M(x,y)\cos[\phi(x,y)] \tag{2}$$

where $I_0(x,y)$, $I_M(x,y)$ and $\phi(x,y)$ are three unknown distributions referred to as the background intensity, the intensity modulation and the phase difference between the

interfering beams respectively. In order to evaluate the phase $\phi(x,y)$, it is therefore necessary to have at least three independent measurements of the intensity $I(x,y)$. A simple and widely used phase evaluation algorithm is based on four intensity measurements where a $\pi/2$ phase shift is introduced between the interfering beams between consecutive interferograms.

The process of recovering the continuous phase distribution $\phi(x,y)$ that extends beyond the $[-\pi, +\pi)$ range is known as phase unwrapping, and consists of adding an appropriate integer multiple of 2π at each point in the wrapped phase distribution (Huntley 2001; Ochoa *et al.* 1998).

When the interferometer is set up to measure object deformations, two phase distributions $\phi_r(x,y)$ (phase of the reference state) and $\phi_d(x, y)$ (phase of the deformed state) are required to evaluate the unwrapped phase change distribution $\Delta\phi(x,y)$.

In this paper we use an alternative method that facilitates low-pass filtering to reduce phase noise (Huntley 2001). In the case when the interferometer has pure out-of-plane sensitivity, i.e. parallel to the observation direction, the relationship between the measured unwrapped phase change $\Delta\phi(x,y)$ and the displacement (or deflection) distribution is given by

$$\delta(x, y) = \frac{\lambda}{4\pi}\Delta\phi(x, y), \tag{7}$$

where λ is the wavelength of the coherent light source used. Eq. (7) assumes that the object and the interferometer are immersed in a medium of unit refractive index.

2.3 Evaluation of film stress from displacement field measurements

Ideally, a film and substrate system such as the one described in Section 2.1 will respond to a uniform stress field in the film by deforming with axial symmetry so that the deflection perpendicular to the plane *x*-*y* has circular contour lines. However, slight heterogeneities in the stress field lead to elliptical contour lines, as shown in Fig. (7). The principal axes of the elliptical contour lines correspond to the directions of the principal in-plane stress components in the film plane.

The deflection distribution $\delta(x,y)$ can conveniently be approximated by a second order surface as follows

$$\delta(x,y) \cong ax^2 + by^2 + cxy + dx + ey + f \,, \tag{8}$$

where the quadratic coefficients a, b and c reflect the curvature characteristics of the paraboloid, while coefficients d and e describe a linear tilt and f the displacement of the centre of mass of the film/substrate system perpendicular to the plane x-y. The linear and constant terms in Eq. (8) can be ignored as they do not contribute to the curvature and therefore are not linked to the film stress. After a convenient change to polar coordinates, Eq. (8) reduces to

$$\delta(r,\theta) \cong r^2\left[a\cos^2\theta + b\sin^2\theta + c\cos\theta\sin\theta\right]. \tag{9}$$

The benefit of this is that once the orientation of the ellipse is determined, the problem is reduced to the determination of δ along the major and minor axes of the ellipse corresponding to θ_M and θ_m respectively. θ_M and θ_m are the rotation angles of the major and minor axes respectively, where

$$\theta_M = \theta_m + \pi/2. \tag{10}$$

Substitution of Eq. (9) into Eq. (1) for θ_M and θ_m finally leads to the film principal stresses

$$\begin{aligned}
\sigma_1 &= \frac{t_s^3}{3t_f^2(1+t_s/t_f)}\frac{E_s}{(1-\nu_s)}(a\cos^2\theta_m + b\sin^2\theta_m + c\cos\theta_m\sin\theta_m), \\
\sigma_2 &= \frac{t_s^3}{3t_f^2(1+t_s/t_f)}\frac{E_s}{(1-\nu_s)}(a\cos^2\theta_M + b\sin^2\theta_M + c\cos\theta_M\sin\theta_M) \,.
\end{aligned} \tag{11}$$

Due to the fact that a higher film stress would be responsible for the curvature of the substrate on the plane that contains the minor axis of the ellipse and the z axis, σ_1 and σ_2 have been defined here following the usual convention in which $\sigma_1 > \sigma_2$.

If $\delta(x,y)$ is available as a full-field measured deflection distribution, then coefficients a, b and c can be found by least squares fitting of the measured distribution to an elliptical paraboloid. Equation (9) is used to find the orientation θ_m of the minor axis by minimizing the radius at a contour of constant deflection. The orientation θ_M of the major axes is found from Eq. (10) and finally Eq. (11) leads to the film principal stresses along θ_m and θ_M.

3. Experiment

3.1 Optical setup

Figure (2) shows a schematic of the interferometer used to measure changes in the curvature of film/substrate due to variations of relative humidity. A He-Ne laser is used as the coherent light source, providing a vertically polarized 30 mW beam with wavelength λ=632.8 nm. The beam goes through a half-wave plate (HWP) that rotates the plane of polarization before entering a polarizing beam splitter (PBS) that splits the incoming beam in two with orthogonal polarizations the intensities of which can be easily adjusted by rotating the HWP. These beams are then launched into single mode polarization preserving optical fibres, after the reference beam (RB) goes through a pair of opposing glass wedges, one of which is fixed and the other is moved across the beam with an open loop piezoelectric lead zirconate titanate (PZT) transducer to increase the optical path and introduce controlled phase steps. The fibres then deliver both beams with the same polarization to the recombination head of the interferometer. The object beam, OB, is transmitted through a non-polarizing beam splitter (NPBS) and propagates towards the film/substrate sample, at which point it is reflected back from the specular bottom surface of the substrate. On its way back, the object beam is recombined with the reference beam so that the optical path difference remains within the coherence length of the laser. A CMOS camera C (HCC-1000 Vosskühler, 8 bits, 1024×1024 pixels) records the interference fringe patterns that encode the shape of the substrate relative to the reference wavefront. The purpose of lens L_1 is to illuminate the sample with a collimated beam, and thus the distance from the tip of the object optical fibre is equal to the focal length of L_1. L_2 collimates the beam launched by the reference fibre and lens L_3 focuses it at the aperture stop plane of imaging lens L_4. This results in a reference beam that covers the CMOS detector with a Gaussian distribution that is typical of the TEM_{00} mode.

As mentioned in Section 2.2 the four-frame algorithm requires, for each deformation state, the acquisition of four interferograms with $\pi/2$ phase shifts between successive ones. A PZT driver is used to generate a calibrated stepped voltage staircase profile $V_1 = 0 < V_2 < V_3 < V_4$ which is stored in a look-up table in the driver's internal microprocessor. During synchronisation, the camera is used as master and the PZT driver as slave. Once triggered from a PC-based application to start the acquisition of four frames, each time the camera records a frame it outputs a TTL rising edge which

is detected by the PZT driver. The driver then moves to the next voltage level in the look-up table and holds it until it receives another TTL rising edge from the camera. Once four steps V_1, V_2, V_3 and V_4 are scanned, it resets to $V_1 = 0V$ ready for the next voltage profile. PZT actuators are sensitive to temperature and for this reason, they need to be calibrated before each measurement, and the laboratory to be temperature controlled. We followed the procedure described by Ochoa (Ochoa *et al.* 1998) to calibrate our PZT phase shifting actuator. The sign of the phase change distribution evaluated through the four-frame algorithm as expressed in Eq. (5) was checked for consistency by simply moving a test object towards the camera, and defining the z-axis accordingly. A calculated positive phase change, corresponding to a positive displacement with the z-axis so defined, is obtained when the object moves towards the camera along the observation direction.

3.2 Preparation of non-aged and UV-aged *urushi* films

The lacquer used in this study was kijiro *urushi*, from Watanabe Syoten Co., Japan. It was first filtered in the traditional Japanese way by filtering the *urushi* through Rayon paper. As *urushi* is an unstable water-in-oil type emulsion, the water soluble polysaccharides in the raw *urushi* can often aggregate during curing (Obataya *et al.* 2002). In order to avoid this, raw *urushi* was mixed and homogenized for about 3 minutes. During this process, gentle mixing is required to prevent the formation of air bubbles. A spin coating machine was used to produce thin films of *urushi* onto circular glass substrates (BK-7, 22 mm diameter and 190 μm ±5 μm thickness). Films with a thickness of around 20 μm were obtained by spin coating at 3000 rpm during 90 s at room temperature. The back surface of the glass substrate was coated with nickel chromate in a vacuum deposition chamber to increase its reflectivity and thus obtain high visibility interference fringes. Immediately after spin coating, the films were cured at 75±2% RH. For films of around 20 μm, it takes at least 3 days to ensure that they are fully cured. The film thickness was measured by focusing a microscope (BX-60 Olympus with 50× objective) on the glass/*urushi* and the *urushi*/air interfaces and measuring the distance required to refocus. We obtained films with a thickness of 21 μm ± 2 μm, which resulted in a film/substrate thickness ratio of about 0.11.

The process just described was used to produce “non-aged” urushi films, without subjecting them to any form of subsequent degradation. One subset of the non-aged

urushi films was then exposed to UV radiation in order to simulate UV aging and observe its effect on the stress response to changes in RH. The UV radiation exposure history of the Mazarin chest is unknown and therefore any attempt to try to replicate its accumulated aging will be flawed. The only clear data on its exposure is that during the period between 1986 to 1998 it was displayed at the Toshiba Gallery in the V&A, London, where the illuminance was 80 lux, with UV levels less than 5 $\mu W.lumen^{-1}$, resulting in an energy density of 0.0004 $W.m^{-2}$. Considering 52 weeks per year, 5 days per week and 8 hrs per day display, this results in a total UV exposure of about 36 $kJ.m^{-2}$. As a comparison, one can estimate the average (accounting for seasonal and daily variations) exposure to 340nm UV radiation due to sunlight as 0.08 $W.m^{-2}$. To induce UV damage, we used a Q-Sun environmental test chamber, equipped with a Xenon arc source, into which the film was exposed to 340 nm, 0.7 $W.m^{-2}$ UV radiation for 400 hrs. Although we do not try to make a direct comparison with conditions that the Mazarin Chest was subjected to, and nor do we try to replicate the damage exactly, in order to place our tests into context, we can calculate that our test protocol is equivalent to an average daylight exposure of 0.4 years or an exposure within the Toshiba gallery of 80 years (assuming 80 lux at 340 nm, though the exposure at this wavelength is likely to be much lower in reality).

3.3 Environmental chamber

Triggering the response of *urushi* films to changes in relative humidity and measuring it with the interferometer requires a fine control over the environmental conditions. An environmental chamber (EC) with thermal and humidity control systems was built. After some trial and error, humidity control was obtained by using a water reservoir within the chamber that was open or closed to the chamber according to the humidity detected by a capacitive sensor. The temperature was maintained using a monitored heating element controlled using a thermocouple transducer. This approach allowed us to control RH and temperature to within ±1% RH and ±1 °C, respectively.

The film/substrate test sample sat horizontally on a recessed holder by its own weight. A steering mirror was used in the object beam as shown in the insert in Fig. 2 to direct it vertically so that the bottom surface of the substrate acted as a specular surface, the shape of which is measured with the interferometer described in Section 2.2.

3.4 Experimental errors

The greatest challenge in this experimental study was to maintain interference fringe stability during the long recording times required for the measurements. Environmental vibration and temperature variations introduce strain in the optical fibres, which can result in relative phase shifts and induce slow fluctuations of the dc component of the measured phase change $\Delta\phi$. To overcome these problems, the interferometer was setup on a vibration isolated table, the room temperature was kept at 18 °C and the optical fibres were thermally insulated. To avoid the effects of changes in room temperature and humidity we regularly recalibrated. Slight rigid body motion of the sample over the sample holder was dealt with in the data processing stage, by following the procedure described in Section 2.3.

The measured optical phase difference maps have some spatial noise which is a combination of electronic noise sources in the camera, camera dynamic range (8 bits in this case), the phase shifting algorithm used, spurious diffraction patterns and also environmental stability. This noise directly affects the measured displacement field δ, which is simply proportional to the phase as expressed by Eq. (7). A common parameter that describes this noise is the root mean square error of the displacement distributions, which is defined as

$$rms = \sqrt{\frac{\sum_{x=1}^{N}\sum_{y=1}^{M}\left(\delta_{\exp}(x,y) - \delta_{fit}(x,y)\right)^2}{N \times M}}, \tag{12}$$

where $\delta_{exp}(x,y)$ is the measured displacement map, $\delta_{fit}(x,y)$ is its best second order polynomial fit and $N \times M$ is the total number of pixels in the region where *rms* is evaluated. It was observed that the *rms* error was below 1.4 μm for t between t_{c1} and the time at which the stress peaked, corresponding to 1% of the maximum deflection at peak stress. For small deformations of the glass substrate, this error is mainly due to the high spatial frequency nature of the phase noise. For large deformations of the substrate, i.e. at peak stress, the *rms* error was at most 1.4 μm for the biggest RH step from 75% to 30%, and reflects not only the spatial variations of the measured displacements but the truncation error of the second order polynomial used to approximate what in reality is not exactly a parabolic displacement field.

We calculated the uncertainty in the average film stress σ from the uncertainties in the substrate thickness $u_{\sigma t_s}$, the film thickness $u_{\sigma t_f}$, the displacement $u_{\sigma\delta}$ and the distance from the centre to where the displacement is measured, $u_{\sigma r}$ by the usual statistical error propagation formula.

where u_{t_s}, u_{t_f}, u_δ and u_r are the uncertainties in t_s, t_f, δ and r, respectively. We neglected the uncertainty in the Young's modulus and Poisson's ratio of glass as these are not tabulated for our substrates. The total error in σ is obtained by combining the individual contributions in quadrature

$$u_\sigma = \sqrt{u_{\sigma t_s}^2 + u_{\sigma t_f}^2 + u_{\sigma\delta}^2 + u_{\sigma r}^2} \tag{17}$$

where u_{t_s}, u_{t_f}, u_δ and u_r are the uncertainties in t_s, t_f, δ and r, respectively. To obtain an estimate of the error associated with the calculated stress, an error propagation analysis was performed using non-aged *urushi* film with the maximum applied RH change from (75% to 30%, resulting in a maximum stress of 121.3MPa, Section 4), using the experimental parameters u_{t_s} = 5 μm, u_{t_f} = 2 μm, u_δ = 1.9 μm, u_r = 0.03 μm, t_s = 190 μm, t_f = 21 μm, δ = 153.8 μm and r = 9 mm. The individual contributions obtained from Eqs. (13-16) to the overall uncertainty u_σ are shown in Table 1. It can be observed that the film thickness t_f has the greatest contribution to the error of the estimated average film stress while the displacement δ and the distance from the centre to where the displacement is measured, r, have the lowest contributions. The overall uncertainty is then approximately 11 MPa, for the state described, suggesting we should expect errors of the order of less than 10 % of the absolute stress observed.

4. Response of urushi to changes in moisture

Figure (4) shows the wrapped phase of difference map, $\Delta\phi_w(x,y)$, for non-aged *urushi* film during exposure to 30% RH after 4080 min. Using Eq. (7), the displacement distribution, $\delta(x,y)$, can be extracted and is shown in Fig. (5). Figure (6) shows the best fit of Eq. (8) to the experimental data, only showing the quadratic coefficients a, b and c. A contour representation of the displacement distribution, Fig. (7), shows the substrate deflection field where the orientation of the minor axis, θ_m, is 2.36 rad and

the orientation of the major axis, θ_M, is 3.93 rad. For this figure, the depth-averaged film stresses along the minor and the major axes, σ_1 and σ_2, are 88.4 MPa and 73 MPa respectively.

The stress response of three non-aged and three UV-aged *urushi* films to changes in RH were measured in this work. All the samples were prepared as described in section 3.2. Each of them was used for measuring its response to two changes in RH, rather than using the same sample to measure different RH changes, so as to avoid history dependent effects. The RH history of each of the samples is shown in Fig. (3). Initially, all samples were kept at the relative humidity for curing, RH_C=75±2%, for 3 weeks to ensure equilibrium. Each sample was then exposed to a step reduction in RH, to one of three different low relative humidity levels, denoted as RH_1 in Fig. (3). Under each low relative humidity level, the film stress was observed over 66 hours, a time that corresponds to 95% of an approach to the asymptote. The measurements were carried out every 5 minutes until the stress reached a maximum value and then every 1 hour. During all measurements the temperature was held constant at 23 °C.

Figures (8a-c) show the development of film stress in three different non-aged and aged *urushi* films during exposure to the low relative humidity levels, as a function of time. The general behaviour of the *urushi* film subsequent to a reduction in humidity from 75% is a positive deflection of the substrate (cusp towards the camera) which corresponds to a tensile in-plane stress developing in the film. This stress peaks within about 2 hrs then relaxes over a longer time scale with a slight reduction in the magnitude of the stress. In order to compare the behaviour of the *urushi* to changes in humidity we plot three functions. Firstly we estimate the rate at which the stress develops in the period after the first step change in humidity occurs (Fig. (9)). Secondly, we note the peak compressive in-plane stress (Figs. (10). Finally we determine the asymptotic stress values (σ_∞) reached in the film (Tables 2-3) by assuming that at long times, that the relaxation function can be modelled by a single relaxation function and fitting an exponential approach to the long time behaviour, approximated by

$$\sigma = \sigma_\infty - \sigma_B \, e^{\left(-t/\tau\right)} \tag{18}$$

where σ_B and τ are fitting constants. We can attribute different physical mechanisms to the stages of deformation for the material when subjected to a reduction in relative

humidity. Shortly after the humidity is changed, the desorption of water will lead to volume shrinkage and as a result of the adhesion to the glass substrate a compressive in plane stress and its associated bending moment will be created. Following this period we observe that compressive in-plane stress peaks after which there is a relaxation of the material. We believe that the most likely explanation for this behaviour is that the viscoelastic properties of the *urushi* lead to time dependent behaviour since the humidity and therefore hygral strain, is maintained at a constant value once hygrothermal equilibrium is reached. We may therefore be observing an effect of stress relaxation in the material. In order to identify the physical processes, further investigation is required to quantify the moisture dependent material properties of *urushi*. The peak stress values and times for non-aged and aged *urushi* samples which were subjected to low relative humidity levels are shown in Tables 2 and 3 and are plotted in Fig. (10) as a function of the difference between storage (75%) and different low RH levels. This shows clearly that the absolute value of the in-plane stress scales with the size of the RH change. Figure (9) shows the rate at which the compressive stress develops in non-aged and aged *urushi* films as a function of the difference between storage (75%) and different low RH levels. As shown in Fig. (9), the stress develops quickly with a change in humidity but it is not clear that the rate increases when the RH difference is made larger.

When the *urushi* films are subjected to an increase in relative humidity (RH_1 to RH_2), a similar behaviour to that seen during desorption is observed. Due to water ingress, we naturally anticipate that there will be a volume increase, and a compressive in-plane stress is observed that supports this. Similar to that observed for desorption, we observe an initial region of rapid in-plane stress change, followed by a peak and relaxation to the asymptotic value. In this case however, the magnitude of the relative humidity changes are small, and the behaviour is correspondingly weaker (Fig. (11a-c)). Semi-log (lin-log) plots have been inserted in Fig. (8) and Fig. (11) to illustrate the stress behaviour during the first 2 hrs when *urushi* subjected to low and high humidity levels.

The behaviour observed following a humidity change is broadly consistent regardless of whether the material has been aged or not. The patterns we observe are similar, but we do observe significant differences in the absolute values. In general, for large reductions in relative humidity, the aged films exhibit a smaller in-plane stress than

the non-aged materials. For example, we observe a ~30% reduction in the peak compressive stress in Fig. (8c), which is replicated for other changes in relative humidity, and applies to the asymptotic stress as well. The picture for the rehydration is much less clear, and it is difficult to obtain good trends from simply looking at the comparisons (Fig. (11c)). For the relaxation following the peak stress, similar behaviour was observed for the asymptotic stresses for the desorption part of the tests (Fig. (8)) however, for the rehydration the in-plane stress changes are much smaller in magnitude and the behaviour is more confused (Fig. (11)). It is likely that these long time trends are highly sensitive to small changes in the environment, and although the conditions remained steady, large fluctuations were observed.

The peak stress values and times for non-aged and aged *urushi* films when going from RH_1 to RH_2 are shown in Table 4. To obtain a better view of the trends when the RH goes from RH_1 to RH_2 the peak stress values and the relative humidity differences for both the aged and the non-aged films are plotted in Fig. (12). We observe different gradients to those observed in Fig. (10), but at this stage, we are unable to determine the physical cause of this phenomenon since the in-plane stress states are different (compressive and tensile) and there is no overlap in the change of relative humidities in the figures.

5. A 1D Model of stress development in urushi layers

Having considered the response of the material to changes in relative humidity, we now propose a 1D model that will be used to characterise and predict urushi behaviour.

5.1 Determination of diffusion coefficient using weight gain experiments

+Description of weight gain experimental procedure.

This procedure was used to determine the moisture uptake for both aged and non-aged *urushi* layers. Using a diffusive model of mass transport we were able to estimate the diffusion coefficient from the weight gain or loss. The mass transport of moisture is described by

$$\frac{\partial \rho}{\partial t} = D \frac{\partial^2 y}{\partial x^2}$$

where an analytical solution to this equation can be obtained in series,

The diffusion coefficient can be obtained from such a solution fitted to the experimental data using regression techniques. The resultant values for diffusion coefficient, and the initial and asymptotic moisture contents are given in Table 5.1. A typical fit is shown in Fig. 5.2. Intermediate moisture contents can be obtained by interpolating the asymptotic moisture content using a quadratic fit and solving for the required moisture content value (Fig. 5.3).

Thus, we are able to then solve the diffusion equation once more, using the initial and asymptotic moisture contents as initial and final conditions, and the fitted D value as our diffusion coefficient, enabling us to determine the spatially varying moisture content values within the layer and subsequently, the depth averaged moisture content, which in Section *, will allow us to calculate the depth average stress in the layer.

5.2 Hygral stresses induced by absorption of moisture

The experimental observations of the stress response over time indicate that the system responds to both changes in moisture content and relaxation of the stresses in the material, with the moisture changes dominating initially, followed by a period in which the relaxation is stronger. Under these conditions, we can consider an isotropic plate in plane stress subject to the biaxial mechanical stresses σ_1 and σ_2, moisture change ΔC and temperature change ΔT. In this case the strain components ε_1 and ε_2 are given by

$$\begin{aligned} \varepsilon_1 &= \sigma_1 / E - \nu\sigma_2 / E + \beta\Delta C + \alpha\Delta T \\ \varepsilon_2 &= -\nu\sigma_1 / E + \sigma_2 / E + \beta\Delta C + \alpha\Delta T \end{aligned} \qquad (1)$$

where α is the thermal expansion coefficient, β is the hygroscopic expansion coefficient, ν is Poisson's ratio and E is Young's modulus. For the case where ε_1, ε_2 and ΔT are all zero, we therefore have the hygral strains $\varepsilon_1^H = \varepsilon_2^H = \beta\Delta C$ assuming

the film is isotropic. The film is however unable to expand due to the underlying substrate, giving rise to hygral stresses $\sigma_1{}^H = \sigma_2{}^H$ where

$$\begin{aligned}\sigma_1{}^H &= \frac{E}{1-\nu}\varepsilon_1{}^H \\ &= \frac{E\beta}{1-\nu}\Delta C\end{aligned} \quad . \tag{2}$$

To describe the stress relaxation over time we employ a three-element viscoelastic material model given by the equation [ref]

$$\begin{aligned}\sigma(t) &= E_\infty \varepsilon_0 \left[1-\exp(-t/T)\right] + \sigma_0 \exp(-t/T) \\ &= E_\infty \varepsilon_0 \left[1-\exp(-t/T)\right] + E_0 \varepsilon_0 \exp(-t/T)\end{aligned} \tag{3}$$

where T is the time constant for the model, ε_0 is the magnitude of the imposed strain step, and E_∞ and E_0 are respectively the relaxed and instantaneous moduli (Ref: 'viscoelasticity of engineering materials', by Y M Haddad). The effective stress relaxation function, R, is therefore

$$R(t) = E_\infty \left[1-\exp(-t/T)\right] + E_0 \exp(-t/T) . \tag{4}$$

The stress for a general strain history, $\sigma(t)$, is

$$\sigma(t) = \int_{-\infty}^{t} R(t-\tau)\dot{\varepsilon}(\tau)d\tau \tag{5}$$

which for the model considered here, with $\sigma(t) = 0$ for $t < 0$, can be written

$$\sigma(t) = \int_0^t \left\{k_1\left[1-\exp(-(t-\tau)/T)\right] + k_2 \exp(-(t-\tau)/T)\right\}\frac{dC(\tau)}{d\tau}d\tau \tag{6}$$

where

$$k_1 = \frac{E_\infty \beta}{1-\nu} \tag{7}$$

and

$$k_2 = \frac{E_0 \beta}{1-\nu}. \tag{8}$$

Thus, the material response to a change in moisture content is characterised by the three parameters k_1, k_2, T, which are themselves combinations of the usual material properties.

The values of k_1, k_2, and T, for each combination of RH and aging can be determined from the experimental data shown in Figs. 5.2 by fitting Eq. (6) to the data. The term dC/dt, proportional to the strain gradient, is calculated by solving the diffusion equation for the experimental conditions (using a Finite-Difference approximation) to obtain the distribution of moisture, determining the depth averaged moisture content as a function of time and then estimating the gradient.

The fitting of Eq. (6) is reasonably good over the time ranges interrogated for all three curves (Figs. 5.4 and 5.5) and rheological parameters, k_1, k_2, and T obtained are shown in Table 5.2. The parameters show no obvious dependency on RH but there does, however, appear to be a systematic upward shift in relaxation time T as the humidity level rises for the non-aged material. For the aged material, the picture is similar, although the data is somewhat confused for the shift from 75% to 42%.

5.3 A 1D model for multiple layers of urushi on a substrate

The agreement between the 1D model and the experimental observation suggests that the important behaviour is being captured by the model. In reality, *urushi* is most often found in multiple layers. A natural extension to the model, therefore, is to incorporate further layers of *urushi*. We consider a domain consisting of two layers of *urushi*, constrained in the lateral direction by the presence of an infinitely stiff and impermeable substrate as the lower most boundary and a completely permeable interfacial layer. The moisture content at the upper most boundary is fixed by the relative humidity in the environment (Fig. 5.6).

The problem is solved in sequential parts. First we solve the diffusion equation using a finite-difference approximation to find the moisture content distribution within each layer. The depth averaged moisture content in each layer is then

calculated from the time-dependent moisture profile. The temporal gradient of the depth averaged moisture content for each layer are then inserted into Eq. (6) and the stress calculated using the material properties k_1, k_2, and T determined previously in Section 5.2.

This model was used to investigate the development of stress as a function of upper layer depth when placed upon a much thicker support layer. The bottom layer was fixed to be 500μm, and represented an aged layer in equilibrium with an environment at 30% RH. We then envisage a scenario where there was a step change in RH resulting in a change of moisture content of 0.2% and determine the stress evolution. Figs. 5.7 show a comparison of the temporal evolution of depth averaged stresses in each layer as a function of the upper layer depth. We see that the stress developed in the upper layer is larger than that in the lower layer. Additionally, we see that the form of the stress function is quite different. The bottom, thick, layer develops stresses increasing monotonically towards an asymptotic value. The stresses in the upper layer, however, respond rapidly to the change in moisture on the top most surface, before relaxing. The thinnest layer shows the largest stresses, but the thinner layers show more complex relaxation. We can attribute this to difference rate at which the upper layer reaches an even distribution of moisture. In thin layers, near-saturation is reached quickly and the diffusion of moisture into the layer is balanced very quickly with the diffusion of moisture across the interface into the lower layer. In the thicker layers however, the moisture distribution continues to develop over much longer timescales resulting in a further slow increase in the stress even after the main relaxation has occurred.

This simple model suggests significant complexity in the stress development in lacquers where conservation may have occurred and the layers are of significantly different age and depth.

6. Conclusions

The stress response of cured non-aged and aged *urushi* films to different humidity levels has been measured using a phase shifting interferometer. This method has been shown to be able to resolve displacements in a bilayer to within 1% of the best second order deflection approximation. We compared the behaviour of aged and non-aged

urushi films when subjected to changes in the environmental relative humidity. We observed similar modes of behaviour, with a strong indication of time dependent behaviour and a coupling of the diffusion and relaxation of the material, but we also observed that the in-plane stresses during desorption were higher for the non-aged *urushi* films and during adsorption were higher for the aged *urushi* films. The results indicate that the material properties are likely to be strongly affected by the moisture ingress during variation of the RH, and this depends on the amount of aging the material has been subjected to. A 1D model has been developed and tested against the experimental observation, showing reasonable agreement. We have demonstrated the potential of our model by investigating the stress response in layers of urushi of varying ages. Further work is required to identify the material constitutive relationships in order to predict and describe *urushi* material behaviour under varying environmental conditions.

Acknowledgements

The authors would like to acknowledge the support of the Victoria and Albert Museum (V&A) and the Toshiba International Foundation (TIFO). AE would like to thank Loughborough University for scholarship contributions. Software developments by Russell Coggrave are gratefully acknowledged.

References

Awazu, K., Yasui, H., Kasamori, M., Ichikawa, T., Funada, Y. & Iwaki, M. 1999 Effect of H-Implantation Energy on the Optical Stability of Implanted Urushi Films under Photo-Irradiation. *Nucl. Instrum. Methods Phys. Res., Sect. B* **148**, 1121-1125.

Cabié, M., Ponchet, A., Rocher, A., Paillard, V. & Vincent, L. 2004 Transmission Electron Microscopy and Raman Measurements of the Misfit Stress in a Si Tensile Strained Layer. *Appl. Phys. Lett.* **84**, 870-872.

Chen, J. & Wolf, I.D. 2003 Study of Damage and Stress Induced by Backgrinding in Si Wafers. *Semicond. Sci. Technol.* **18**, 261-268.

Cheng, Y.Y. & Wyant, J.C. 1985 Phase Shifter Calibration in Phase-Shifting Interferometry. *Appl. Opt.* **24**, 3049-3052.

Clyne, T.W. & Gill, S.C. 1996 Residual Stresses in Thermal Spray Coatings and Their Effect on Interfacial Adhesion: A Review of Recent Work. *J. Therm. Spray Technol.* **5**, 1-18.

Francis, L.F., McCormick, A.V., Vaessen, D.M. & Payne, J.A. 2002 Development and Measurement of Stress in Polymer Coatings. *J. Mater. Sci. Technol.* **37**, 4717-4731.

Huang, S. & Zhang, X. 2006 Extension of the Stoney Formula for Film-Substrate Systems with Gradient Stress for Mems Applications. *J. Micromech. Microeng.* **16**, 382-398.

Huntley, J.M. 2001 Automated Analysis of Speckle Interferograms. In *Digital Speckle Pattern Interferometry and Related Techniques* (ed. P.K. Rastogi), pp. 59-139. Chichester: John Wiley & Sons Ltd.

Kandil, F.A., Lord, J.D., Fry, A.T. & Grant, P.V. 2001 A Review of Residual Stress Measurement Methods - a Guide to Technique Selection. National Physical Laboratory Report MATC, Teddington, UK.

Kim, J.G. & Yu, J. 1998 A Study on the Residual Stress Measurement Methods on Chemical Vapor Deposition Diamond Films. *J. Mater. Res.* **13**, 3027-3033.

Klein, C.A. 2000 How Accurate Are Stoney's Equation and Recent Modifications. *J. Appl. Phys.* **88**, 5487-5489.

Kumanotani, J. 1995 Urushi (Oriental Lacquer) - a Natural Aesthetic Durable and Future-Promising Coating. *Prog. Org. Coat.* **26**, 163-195.

Lu, J. 1996 *Handbook of Measurement of Residual Stresses*, 1st edn, pp. 71-149. Lilburn: The Fairmont Press, Inc.

Lu, R. & Yoshida, T. 2003 Structural and Molecular Weight of Asian Lacquer Polysaccharides. *Carbohydr. Polym.* **54**, 419-424.

Malacara, D., Servin, M. & Malacara, Z. 2005 *Interferogram Analysis for Optical Testing*, 2nd edn, pp. 493-504. Boca Raton, FL: Taylor & Francis Group, LLC.

Matejicek, J. & Sampath, S. 2003 In Situ Measurement of Residual Stresses and Elastic Moduli in Thermal Sprayed Coatings: Part 1: Apparatus and Analysis. *Acta Mater.* **51**, 863-872.

Obataya, E., Furuta, Y., Ohno, Y., Norimoto, M. & Tomita, B. 2002 Effect of Aging and Moisture on the Dynamic Viscoelastic Properties of Oriental (Urushi) Film. *J. Appl. Polym. Sci.* **83**, 2288-2294.

Ochoa, A. & Huntley, J.M. 1998 Convenient Method for Calibrating Nonlinear Phase Modulators for Use in Phase-Shifting Interferometry. *Opt. Eng.* **37**, 2501-2505.

Ogawa, T., Arai, K. & Osawa, S. 1998a Light Stability of Oriental Lacquer Films Irradiated by a Fluorescent. *journal of environmental polymer degradation* **6**, 59-65.

Ogawa, T., Inoue, A. & Osawa, S. 1998b Effect of Water on Viscoelastic Properties of Oriental Lacquer Film. *J. Appl. Polym. Sci.* **69**, 315-321.

Rivers, S. 2003 *On the Conservation of the Mazarin Chest*. In *27th International Symposium on the Conservation and Restoration of Cultural Property*, Tokyo National Research Institute for Cultural Property/Tokyo National Museum, Japan: 150-158.

Robinson, D.W. 1993 Phase Unwrapping Methods. In *Interferogram Analysis: Digital Fringe Pattern Measurement Techniques* (ed. D.W. Robinson and G.T. Reid), pp. 194-216. Bristol: Institute of Physics Publishing.

Schafer, J.D., Nafe, H. & Aldinger, F. 1999 Macro-and Microstress Analysis in Sol-Gel Derived $Pb(Zr_x\ Ti_{1-X})O_3$. *J. Appl. Phys.* **85**, 8023-8031.

Tien, C.L., Lee, C.C. & Jaing, C.C. 2000 The Measurement of Thin Film Stress Using Phase Shifting Interferometry. *J. Mod. Opt.* **47**, 839-849.

Tsui, Y.C. & Clyne, T.W. 1997 An Analytical Model for Predicting Residual Stresses in Progressively Deposited Coating - Part 1: Planar Geometry. *Thin Solid Films* **306**, 23-33.

Welzel, U., Ligot, J., Lamparter, P., Vermeulen, A.C. & Mittemeijer, E.J. 2005 Stress Analysis of Polycrystalline Thin Films and Surface Regions by X-Ray Diffraction. *J. Appl. Crystallogr.* **31**, 1-29.

Withers, P.J. & Bhadeshia, H.K.D. 2001 Residual Stress-Measurement Techniques. *Mater. Sci. Technol.* **17**, 355-365.

Tables

Table 1. The uncertainty in the average film stress σ due to the substrate thickness t_s, the film thickness t_f, the displacement δ and the distance from the centre to where the displacement is measured, r.

$u_{\sigma t_s}$ (MPa)	$u_{\sigma t_f}$ (MPa)	$u_{\sigma \delta}$ (MPa)	$u_{\sigma r}$ (MPa)	u_{σ} (MPa)
2.4	10.4	1.2	6.2×10^{-4}	10.7

Table 2. Maximum stress, time of peak occurrence, stress rate and the asymptotic stress values obtained for non-aged *urushi* films in response to different amounts of decrease in relative humidity.

RH_C (%)	RH_1 (%)	non-aged *urushi*			
		σ_{max} (MPa)	time (min)	stress rate (MPa.min^{-1})	asymptotic stress values σ_∞ (MPa)
75	30	121.3	100	-2.024	-82.64
75	36	107.1	135	-2.2849	-75.42
75	42	100.1	140	-2.0533	-76.62

Table 3. Maximum stress, time of peak occurrence, stress rate and the asymptotic stress values obtained for aged *urushi* films in response to different amounts of decrease in relative humidity.

RH_C (%)	RH_1 (%)	aged *urushi*			
		σ_{max} (MPa)	time (min)	stress rate (MPa.min^{-1})	asymptotic stress values σ_∞ (MPa)
75	30	85.24	90	-2.431	-62.14
75	36	79.85	115	-2.3274	-63.15
75	42	74.09	100	-1.8778	-54.22

Table 4. Maximum stress and time of peak occurrence obtained for non-aged and UV-aged *urushi* films in response to different amounts of increase in relative humidity.

initial RH_1 (%)	final RH_2 (%)	non-aged *urushi*		aged *urushi*	
		σ_{max} (MPa)	t (min)	σ_{max} (MPa)	t (min)
30	60	108.6	75	125.4	15
36	54	64.98	130	82.26	165
42	48	24.62	120	23.67	600

Table 5.

Humidity change	D / (min/m^2)	$M_c(0)$ / %	$M_c(\infty)$ / %
75%→30%	0.55×10^{-10}	1.6643	0.3521
30%→40%	0.85×10^{-10}	0.3912	0.5658
40%→50%	0.65×10^{-10}	0.6170	0.8367

Table 6. Summary of best-fit viscoelastic model parameters.

Humidity change	k_1 / (MPa%)	k_2 / (MPa%)	T / min
75%→30%	88	126	1676
75%→36%	82	120	1756
75%→42%	142	186	2088

Table 7. Summary of best-fit viscoelastic model parameters.

Humidity change	k_1 / (MPa%)	k_2 / (MPa%)	T / min
75%→30%	64	82	2124
75%→36%	69	85	966
75%→42%	0	89	32863

Figure captions

Figure 1: (a) Deflection of an initially flat substrate due to compressive stress following film shrinkage. (b) A schematic showing the top view of the substrate geometry.

Figure 2: Schematic of phase shifting interferometer and side view of the object beam and the environmental chamber EC: HWP, half-wave plate; PBS, polarizing beam splitter; PZT, open loop piezoelectric transducer; RB, reference beam; OB, object beam; NPBS, non polarizing beam splitter; L_1, L_2 and L_3 convex lenses; L_4, imaging lens; C, CMOS camera.

Figure 3: Schematic of step changes in relative humidity levels with time, where RH_C = 75% is the curing RH, RH_1 is the low RH = 30%, 36% and 42% and RH_2 is the high RH= 60%, 54% and 48%. t_{C1} and t_{12} are the times at which RH changes from RH_C to RH_1 and from RH_1 to RH_2, respectively.

Figure 4: Wrapped phase of difference for non-aged *urushi* film when exposed to a humidity change from 75% to 30% for 4080 min.

Figure 5: Displacement distribution map for non-aged *urushi* film when exposed to a humidity change from 75% to 30% for 4080 min.

Figure 6: Least square fitting of the displacement distribution using the quadratic coefficients for non-aged *urushi* film when exposed to a humidity change from 75% to 30% for 4080 min.

Figure 7: Displacement distribution contour for non-aged *urushi* film when exposed to a humidity change from 75% to 30% for 4080 min.

Figure 8: Film stress development in non-aged and aged *urushi* films after changing the humidity from 75% to (a) 30%, (b) 36% and (c) 42%.

Figure 9: Stress rate in non-aged and aged *urushi* films as a function of the difference between storage (75 %) and different low RH levels.

Figure 10: Effect of relative humidity changes ΔRH (RH_C to RH_1) on the peak film stress developed in non-aged and UV-aged *urushi* films.

Figure 11: Film stress development in non-aged and aged *urushi* films after changing the humidity from (a) 30% to 60%, (b) 36% to 54% and (c) 42% to 48%.

Figure 12: Effect of relative humidity changes ΔRH (from RH_1 to RH_2) on the peak film stress developed in non-aged and aged *urushi* films.

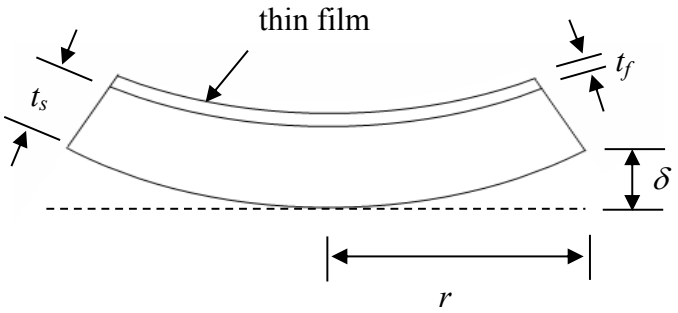

(a)

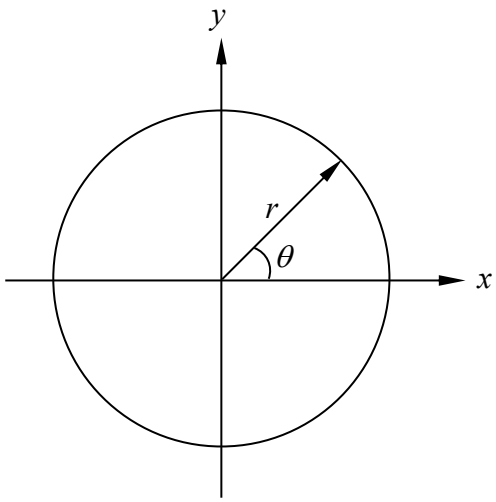

(b)

Figure 1

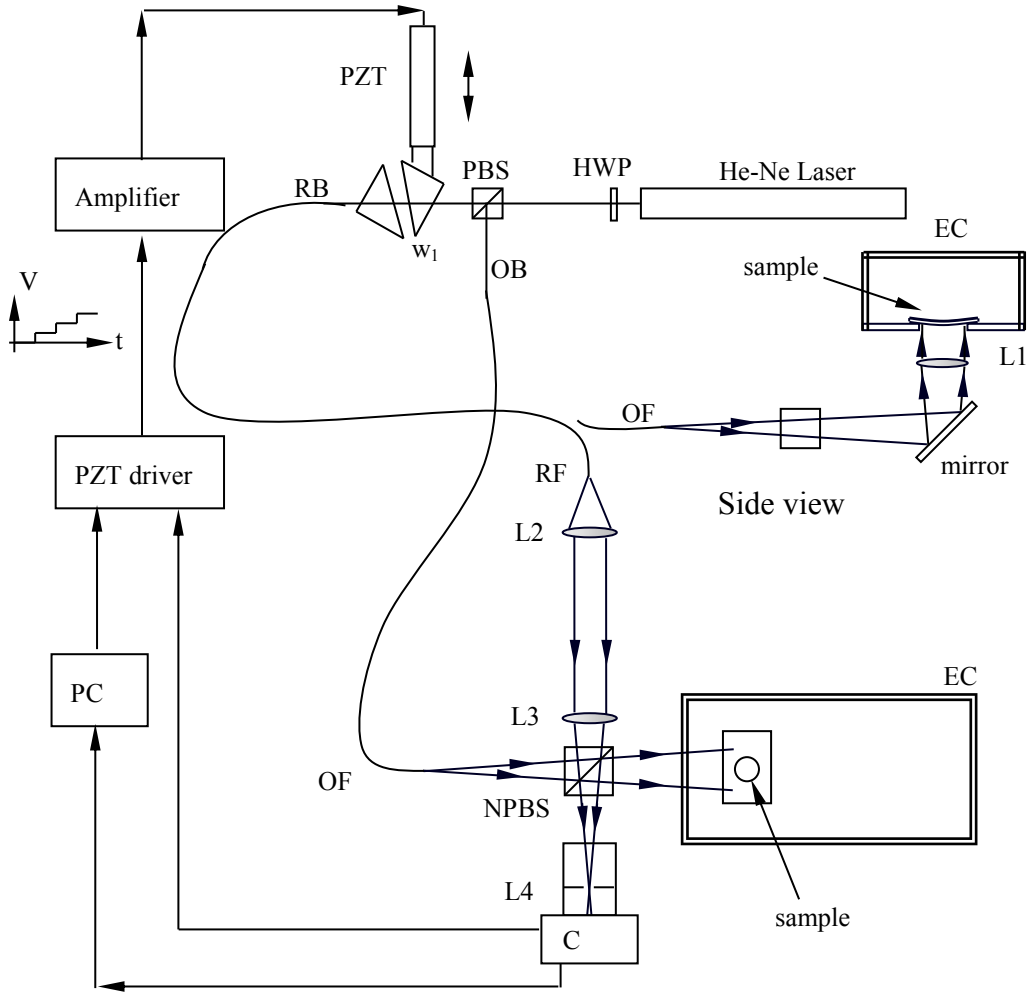
PZT
Amplifier
RB
PBS
HWP
He-Ne Laser
EC
sample
V
t
OB
L1
OF
mirror
PZT driver
RF
Side view
L2
PC
EC
L3
OF
NPBS
L4
sample
C

Figure 2

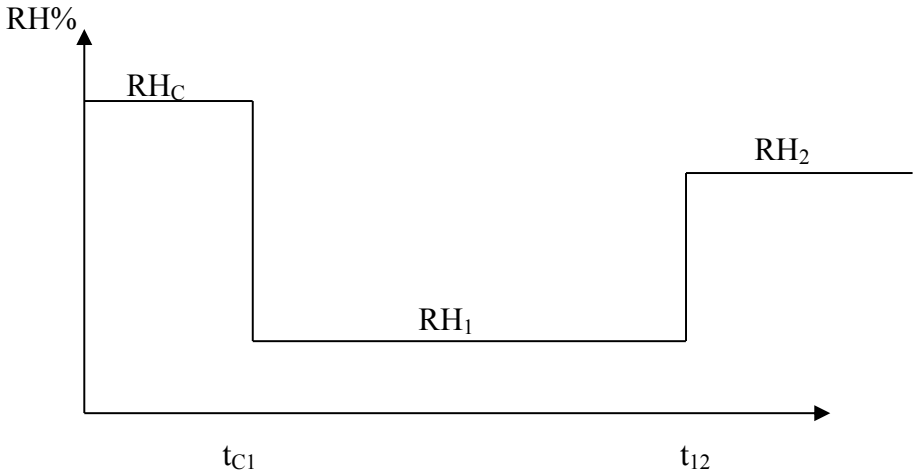

Figure 3

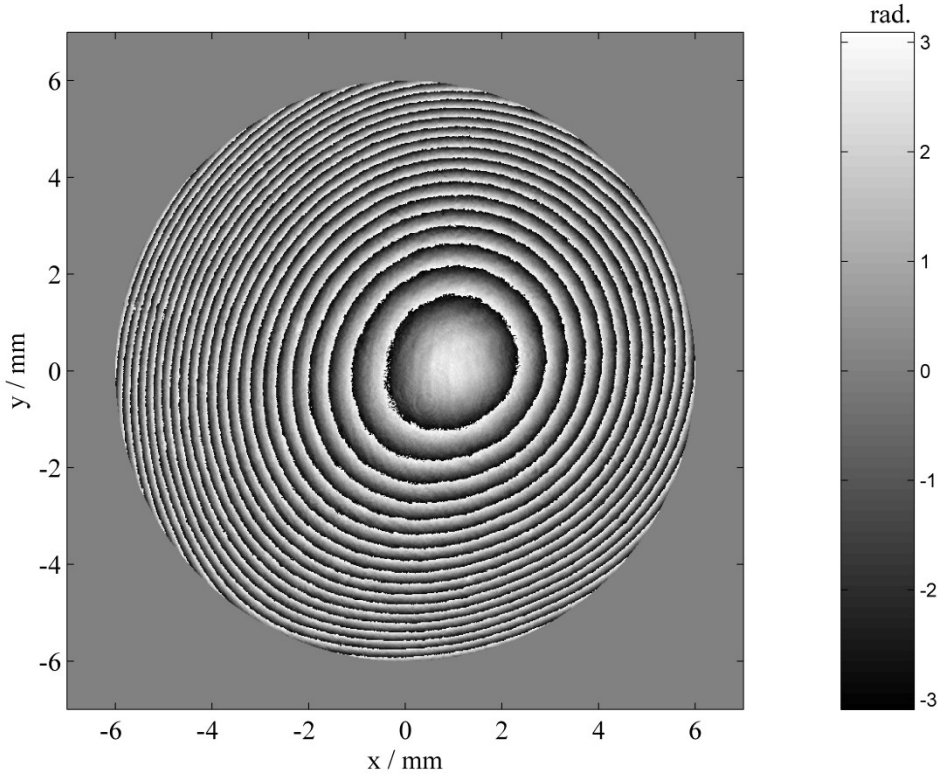

Figure 4

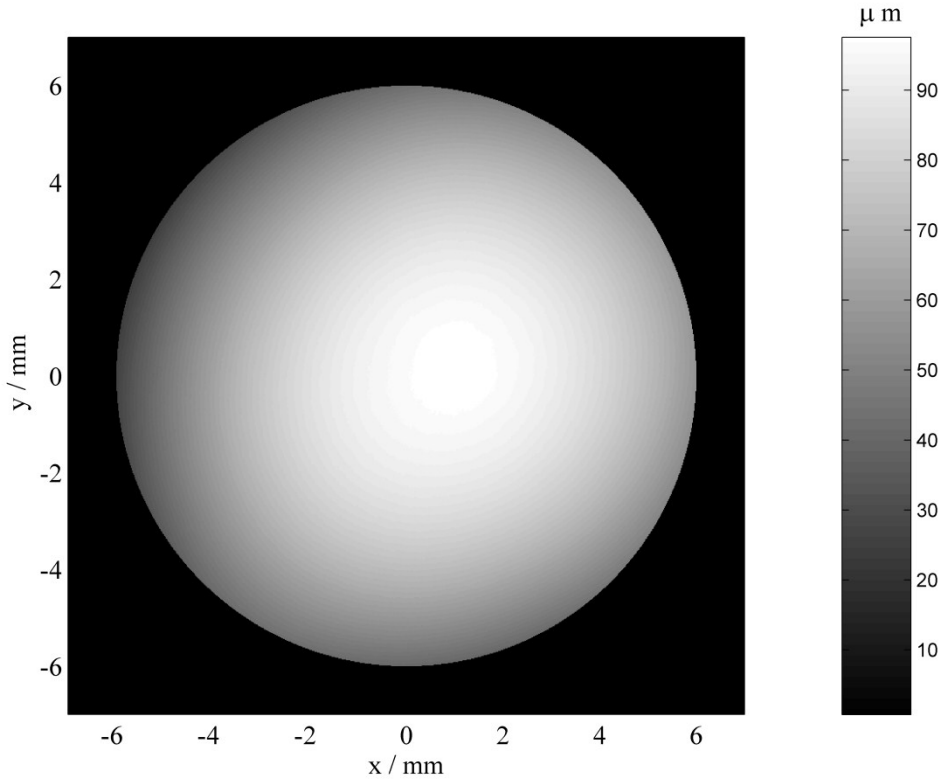

Figure 5

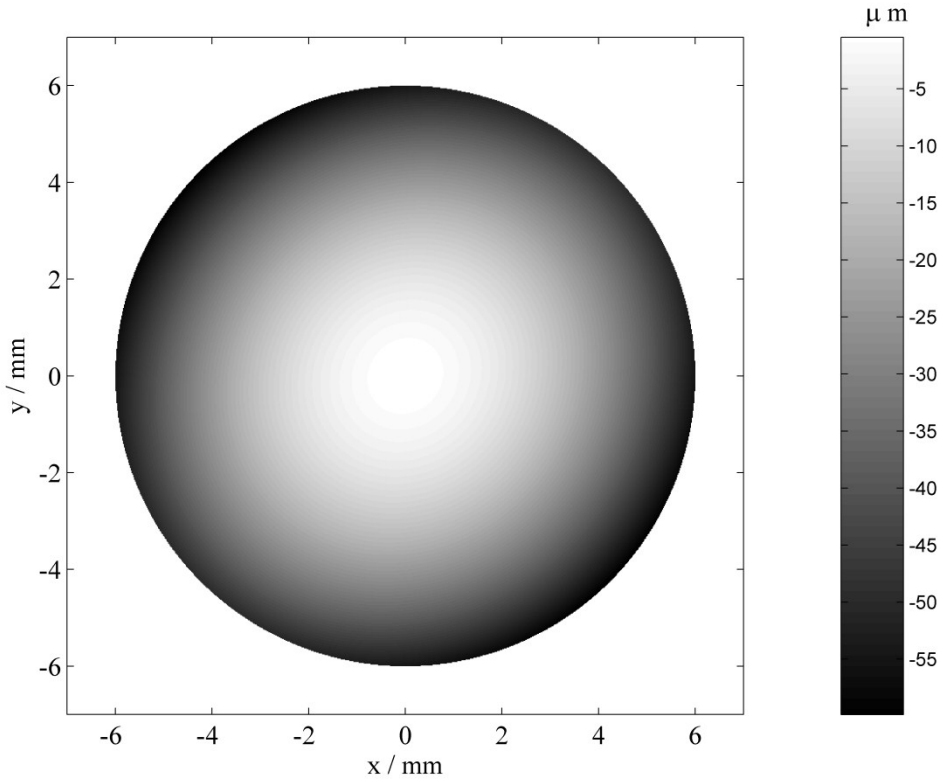

Figure 6

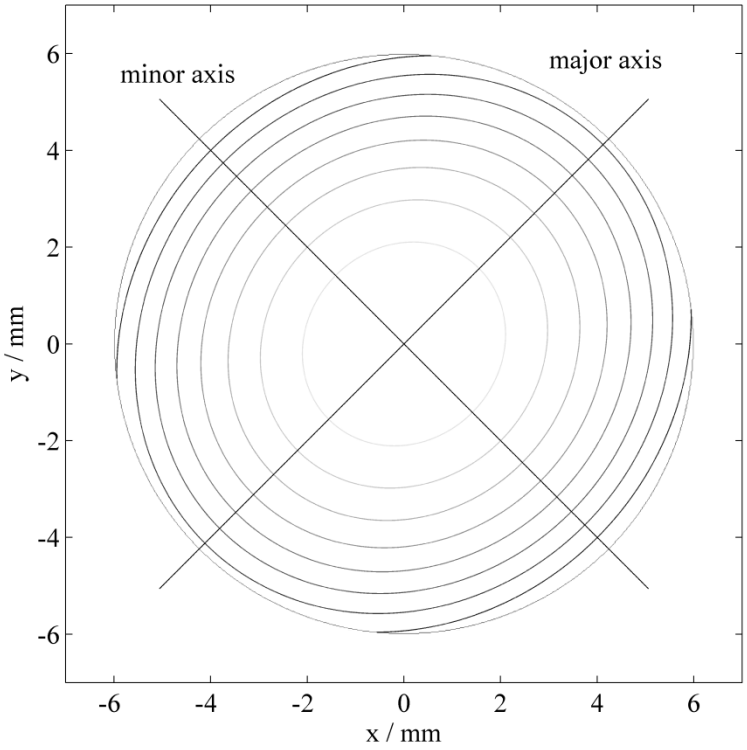

Figure 7

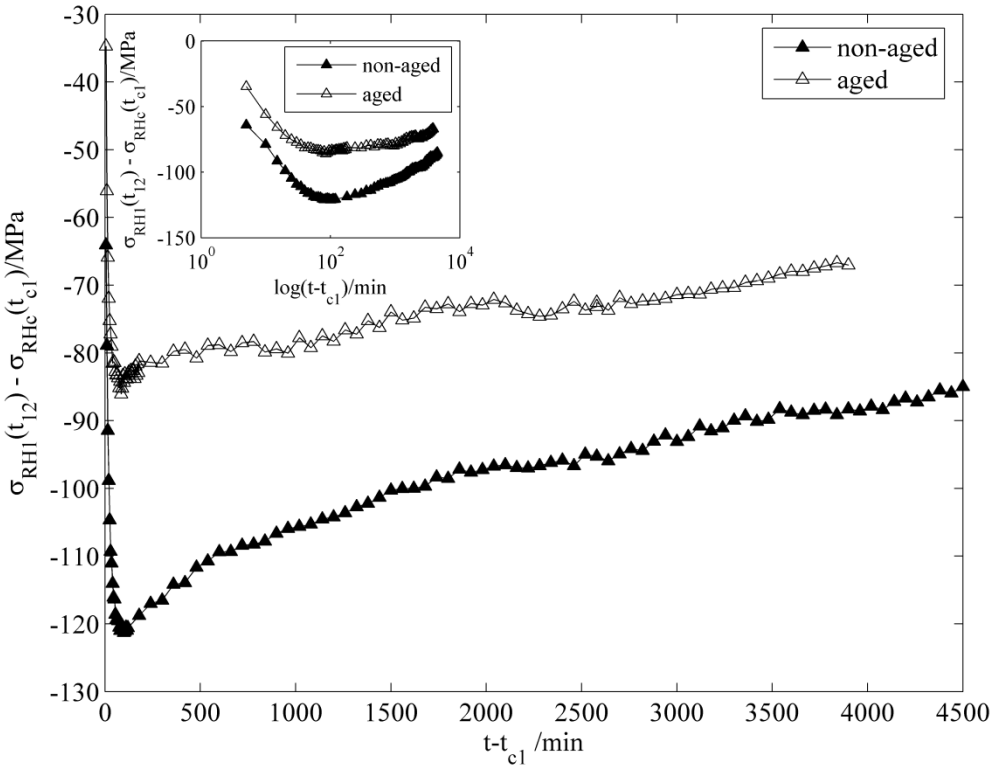
non-aged
aged
$\sigma_{RHl}(t_{l2}) - \sigma_{RHc}(t_{c1})$/MPa
$t-t_{c1}$ /min
$\log(t-t_{c1})$/min

Figure 8 (a)

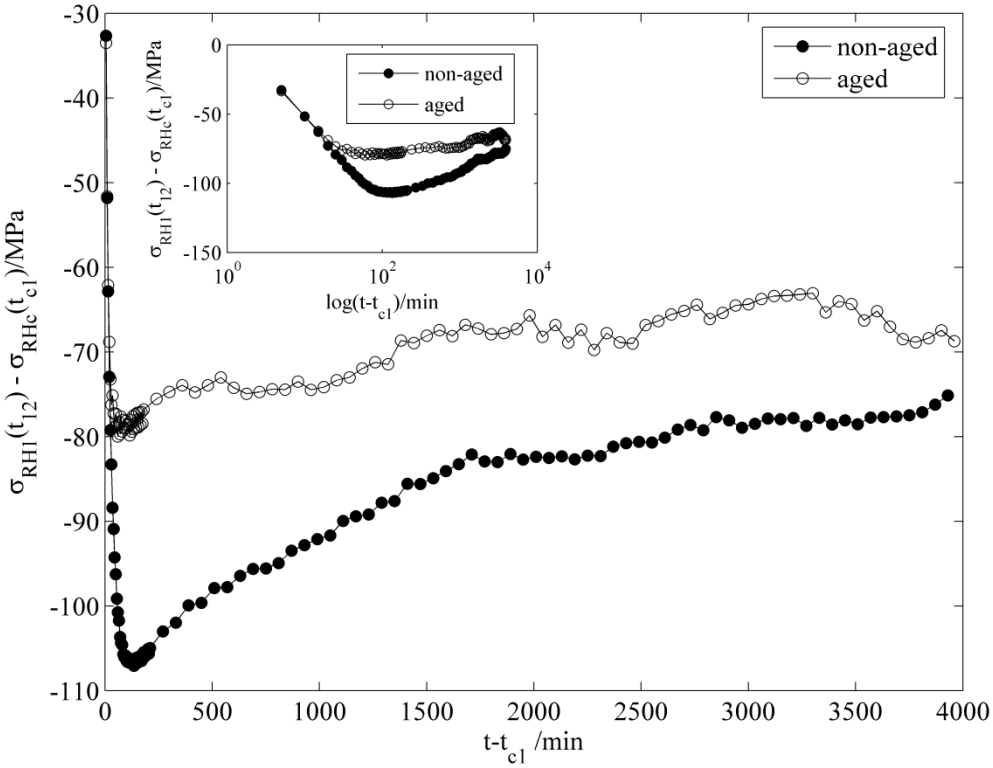
non-aged
aged
$\sigma_{RHl}(t_{l2}) - \sigma_{RHc}(t_{c1})$/MPa
$t-t_{c1}$ /min
$\log(t-t_{c1})$/min

Figure 8 (b)

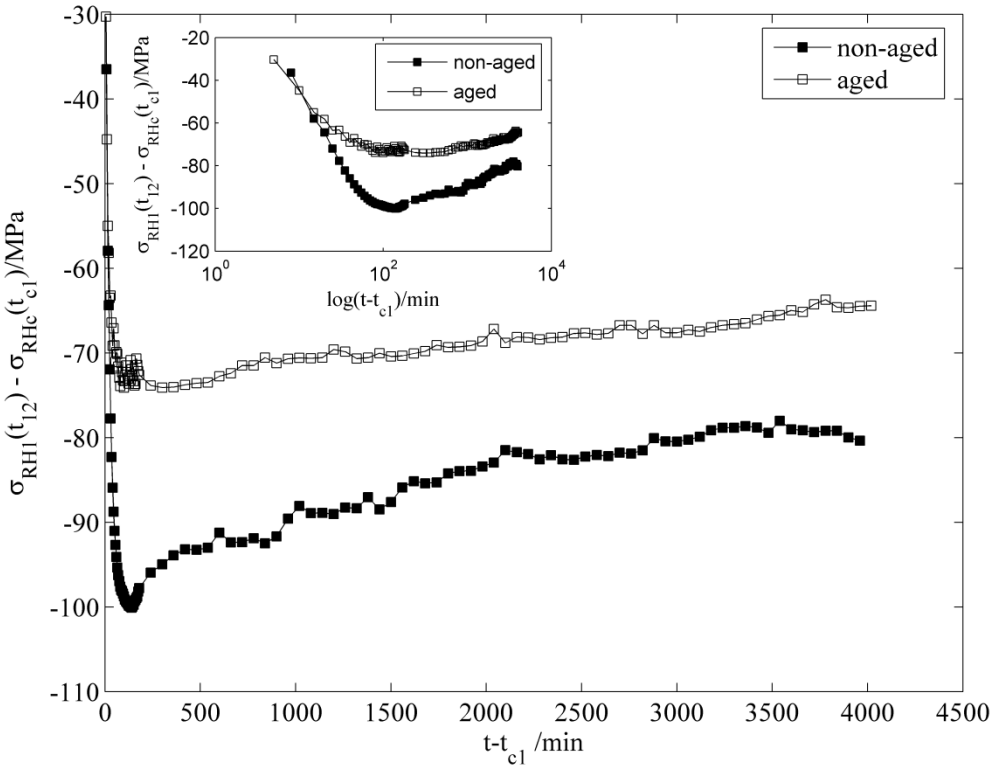
non-aged
aged
$\sigma_{RHl}(t_{l2}) - \sigma_{RHc}(t_{c1})$/MPa
$t-t_{c1}$ /min
$\log(t-t_{c1})$/min

Figure 8 (c)

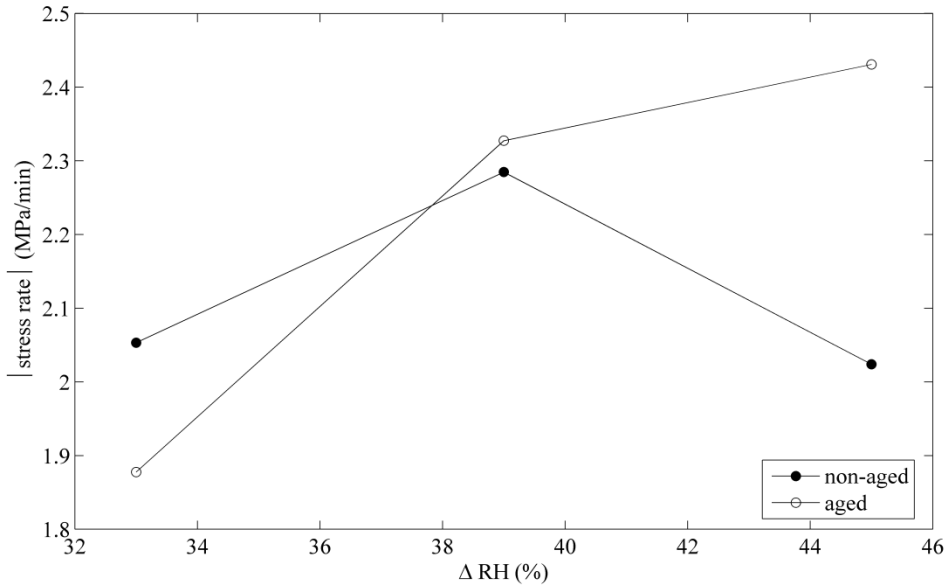
2.5
2.4
2.3
2.2
2.1
2
1.9
1.8
32
34
36
38
40
42
44
46
|stress rate| (MPa/min)
Δ RH (%)
non-aged
aged

Figure 9

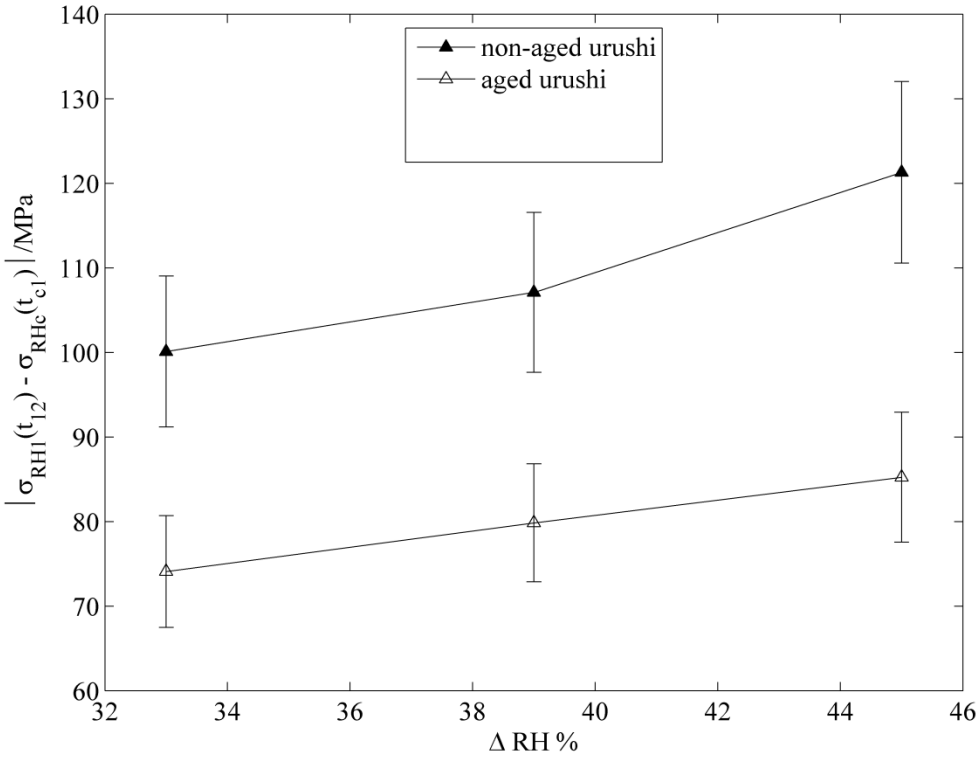
non-aged urushi
aged urushi
$|\sigma_{RHl}(t_{l2}) - \sigma_{RHc}(t_{c1})|$ /MPa
Δ RH %
140
130
120
110
100
90
80
70
60
32
34
36
38
40
42
44
46

Figure 10

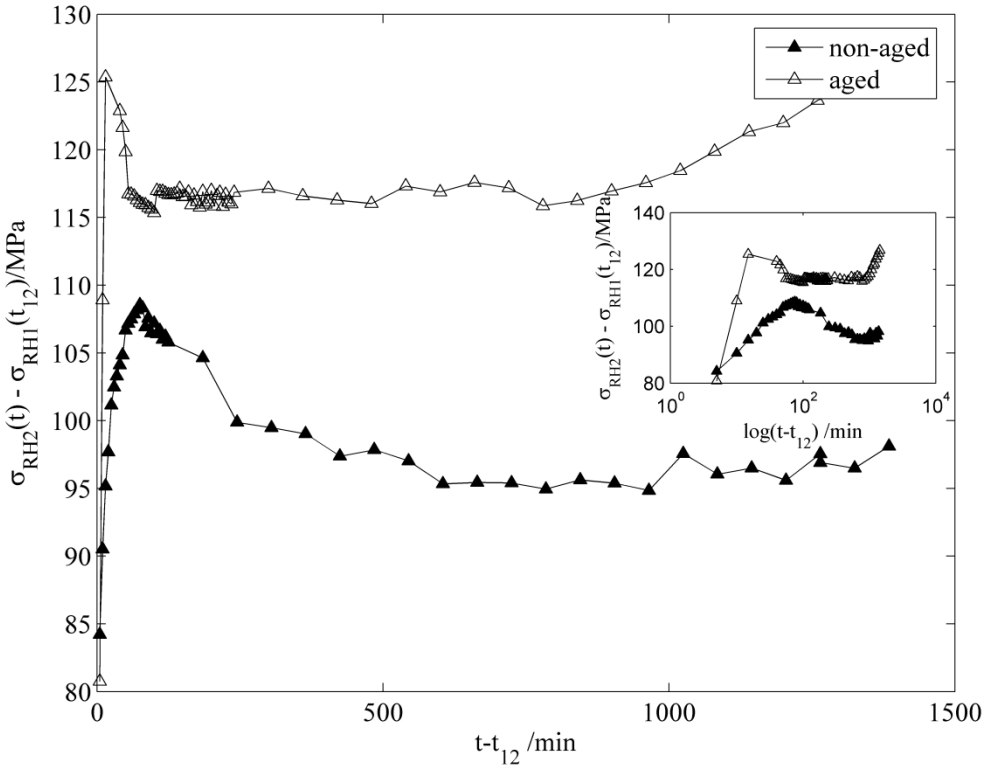
non-aged
aged
$\sigma_{RH2}(t) - \sigma_{RH1}(t_{12})$/MPa
$t-t_{12}$ /min
$\log(t-t_{12})$ /min

Figure 11 (a)

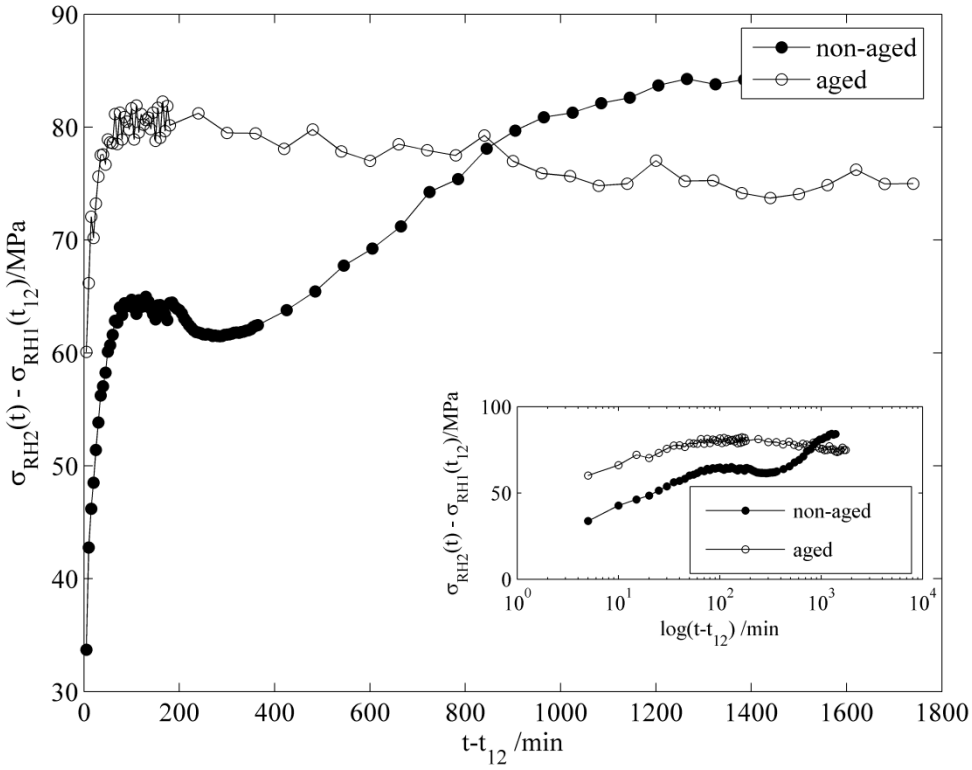
non-aged
aged
$\sigma_{RH2}(t) - \sigma_{RH1}(t_{12})$/MPa
$t-t_{12}$ /min
$\log(t-t_{12})$ /min

Figure 11 (b)

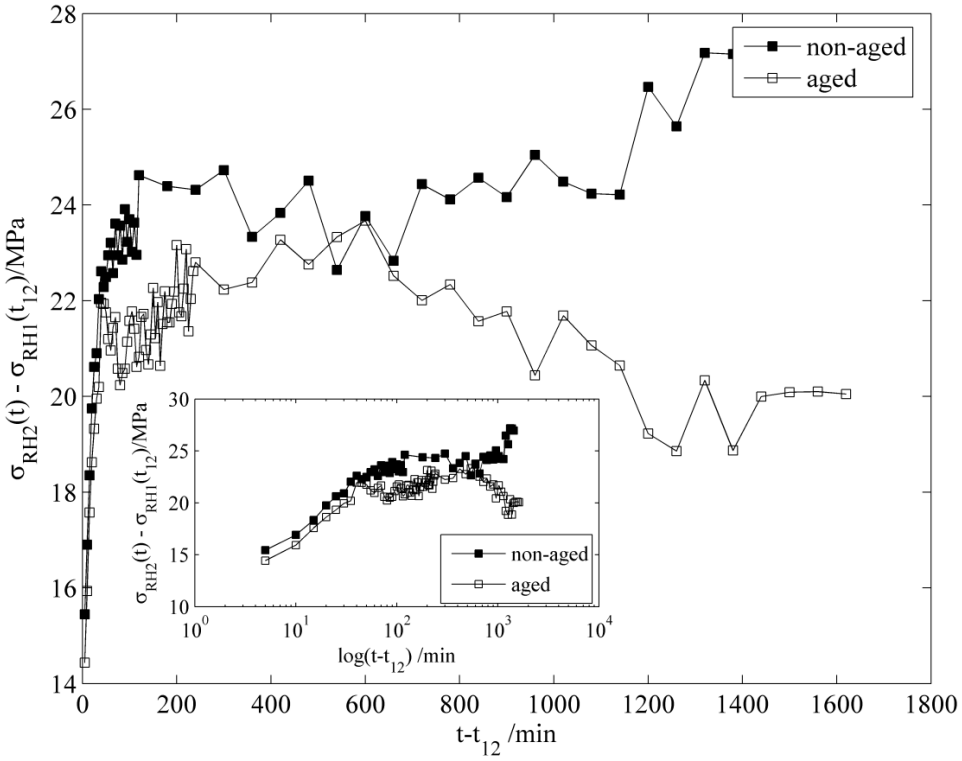
non-aged
aged
$\sigma_{RH2}(t) - \sigma_{RH1}(t_{12})$/MPa
$t-t_{12}$ /min
$\log(t-t_{12})$ /min

Figure 11 (c)

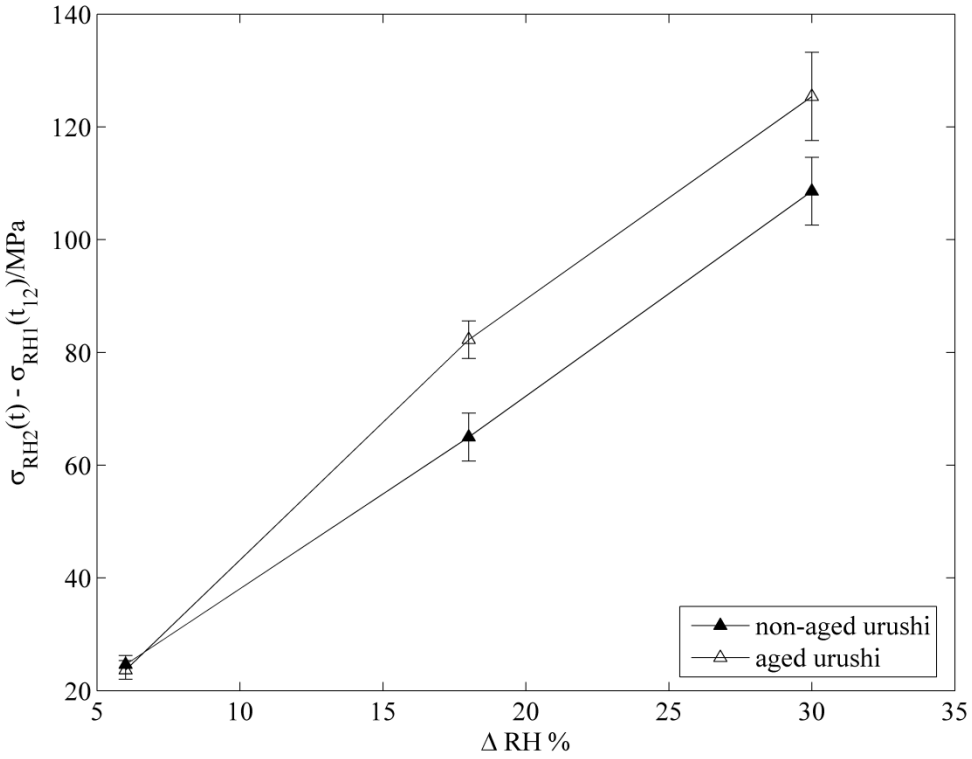
140
120
100
80
60
40
20
5
10
15
20
25
30
35
σRH2(t) - σRH1(t12)/MPa
Δ RH %
non-aged urushi
aged urushi

Figure 12